UC Riverside
UC Riverside Electronic Theses and Dissertations

Title
X-Ray Crystallography of Novel Aryl-Fluorosulfate Lysine Covalent Inhibitor of Apoptosis Protein (IAP) Antagonist

Permalink
https://escholarship.org/uc/item/4dh490hf

Author
Garza Granados, Ana Patricia

Publication Date
2023

Peer reviewed|Thesis/dissertation

eScholarship.org Powered by the California Digital Library
University of California

UNIVERSITY OF CALIFORNIA
RIVERSIDE

X-Ray Crystallography of Novel Aryl-Fluorosulfate Lysine Covalent Inhibitor of Apoptosis Protein (IAP) Antagonist

A Thesis submitted in partial satisfaction
of the requirements for the degree of

Master of Science

in

Biomedical Sciences

by

Ana Patricia Garza Granados

September 2023

Thesis Committee:
Dr. Scott D. Pegan, Chairperson
Dr. Maurizio Pellecchia
Dr. Seema Tiwari-Woodruff

Copyright by
Ana Patricia Garza Granados
2023

The Thesis of Ana Patricia Garza Granados is approved:

Committee Chairperson

University of California, Riverside

ACKNOWLEDGEMENTS

This research was supported in part by the NIH, with grants CA168517 (to MP and SDP, CA242620 (to MP), and NS107479 (to MP). Use of the Advanced Photon Source was supported by the U.S. Department of Energy, Office of Science, Office of Basic Energy Sciences, under Contract W-31-109-Eng-38(SOP). Data for XIAP BIR3 142D6 was collected at Structural Biology Center Collaborative Access Team (SBC-CAT) ID-19 beamline at the Advanced Photon Source, Argonne National Laboratory. Results shown in this report are derived from work performed at Structural Biology Center funded by the U.S. Department of Energy, Office of Biological and Environmental Research and operated for the DOE Office of Science at the Advanced Photon Source by Argonne National Laboratory under Contract No. DE-AC02-06CH11357. Marvin and ChemAxon products were in part used for creation of the chemical linker structure, Marvin 6.2.1, 2014 and supported by ChemAxon (http://www.chemaxon.com)

ABSTRACT OF THE THESIS

X-Ray Crystallography of Novel
Aryl-Fluorosulfate Lysine Covalent
Inhibitor of Apoptosis Protein (IAP) Antagonist

by

Ana Patricia Garza Granados

Master of Science, Graduate Program in Biomedical Sciences
University of California, Riverside, September 2023
Dr. Scott D. Pegan, Chairperson

This thesis presents a comprehensive study on the crystallography of a novel SMAC mimetic, (R)-1-((S)-1-((S)-2-cyclohexyl-2-((S)-2-(methylamino) propanamido) acetyl) pyrrolidine-2-carboxamido) -2,3-dihydro-1H-inden-4-yl sulfurofluoridate, also known as 142D6, and its covalent adduct formation with XIAP BIR3. The inhibitor, 142D6, was designed to simulate the binding properties of Second Mitochondria-derived Activator of Caspases (SMAC) protein, a critical regulator of apoptosis. By utilizing crystallographic techniques, we aimed to elucidate the structural basis of the interaction between 142D6 and XIAP BIR3.

First, a detailed characterization of the crystal structure of 142D6 was performed, revealing its precise and tightly fitted arrangement within the domain subpockets. This structural analysis provided valuable insights into the molecular features of 142D6 that contribute to its binding specificity and potential as an inhibitor.

Furthermore, the covalent adduct formation between 142D6 and XIAP BIR3 determined the complex structure, capturing the precise binding interactions between 142D6 and XIAP BIR3. This analysis highlighted a novel finding, the formation of a covalent bond between 142D6 and XIAP BIR3 Lys299 residue, shedding light on the mechanism of inhibition and the potential for irreversible inhibition strategies. By understanding the structural details of this interaction, we can gain valuable insights into the design of more potent and selective SMAC mimetics for potential clinical applications.

Overall, this thesis provides a comprehensive crystallographic analysis of the novel SMAC mimetic, 142D6, and its covalent adduct formation with XIAP BIR3 at Lys299 residue. The findings presented here enhance our understanding of the structural basis of inhibition and pave the way for the development of improved apoptotic modulators with potential therapeutic application.

TABLE OF CONTENTS

ACKNOWLEDGEMENTS iv
ABSTRACT OF THE THESIS v
TABLE OF CONTENTS vi
LIST OF TABLES vii
LIST OF FIGURES ix
INTRODUCTION 1
1.1 Apoptosis: Programmed Cell Death 1
1.2 Caspase Functions in Cell Death 2
1.3 Inhibitor of Apoptosis Protein (IAP) 4
1.4 Secondary Mitochondria-Derived Activator of Caspase (SMAC) 5
1.5 SMAC Mimetics (SM) 6
1.6 Novel Aryl-Fluorosulfate Lysine Covalent Inhibitor of Apoptosis Protein (IAP) Antagonist 142D6 10
RESULTS 12
2.1 P1 Pocket 14
2.2 P2 Pocket 16
2.3 P3 Pocket 17
2.4 P4 Pocket 19
DISCUSSION & CONCLUSIONS 21
3.1 Opportunities for Improved Efficacy of the 142D6 Scaffold 24
3.2 Concluding Thoughts 29
EXPERIMENTAL SECTION 30
4.1 Crystallization of XIAP BIR3 142D6 30
4.2 Data Processing and Structure Solutions 30
REFERENCES 33

LIST OF TABLES

Table 1. Inhibitor of Apoptosis family nomenclature, common name, and corresponding caspase 5

Table 2. SMAC Mimetic Name and Chemical Structure 9

Table 3. XIAP BIR3 142D6 complex X-ray Data collection and Refinement Statistics. (Molecular Replacement) 32

LIST OF FIGURES

Figure 1. Extrinsic and Intrinsic Apoptosis Pathways 2

Figure 2. Zoomed-in view of apoptosis: SMAC, XIAP, and effector caspases..... 3

Figure 3. Wall-eyed stereo view of 142D6 covalently linked to XIAP BIR3..... 13

Figure 4. XIAP BIR3 P1 pocket interactions with 142D6. 15

Figure 5 XIAP BIR3 P2 pocket interactions with 142D6. 17

Figure 6. XIAP BIR3 P3 pocket interactions with 142D6. 19

Figure 7 . XIAP BIR3 P4 pocket interactions with 142D6. 20

Figure 8. Overlay of monomers A and B from the crystal structure of XIAP BIR3-142D6 complex 21

Figure 9. Proposed S_N2 Sulfur (VI) fluoride exchange (SuFEx) reaction mechanism of 142D6 and XIAP BIR3 23

Figure 10. (A) Schematic representation of the interactions of 142D6 in the BIR3 domain pockets of XIAP. (B) Location of 142D6 into the BIR3 binding pocket. 23

Figure 11. Proposed 142D6 modifications. 23

INTRODUCTION

1.1 Apoptosis: Programmed Cell Death

Apoptosis, or programmed cell death, has become a prominent research area in biomedical sciences due to its correlation with many diseases. Excessive apoptotic activity is related to neurodegenerative diseases, such as Alzheimer's, Parkinson's, and SMA, while insufficient apoptotic activity is related to autoimmune diseases and cancer[1]. The aggressive genetic and epigenetic abnormalities of cancer cells are procured through an accumulation of defects within the signal transduction pathway, proliferation and migration regulation, and apoptotic mechanisms. Various molecular cascades occur in the process of apoptosis via extrinsic and intrinsic cellular pathways[2, 3]. The extrinsic pathway, also known as death receptor-mediated apoptosis, is initiated by extracellular signals prompting death ligand binding to death receptors and plays a crucial role in immune response, development, and tissue homeostasis. The intrinsic pathway, also known as the mitochondrial pathway, causes the release of pro-apoptotic proteins and originates from DNA damage, oxidative stress, or growth factor withdrawal from within the cell. While the two pathways are distinct in terms of their initial signals and proteins, they both ultimately converge on the activation of effector caspases (**Figure 1**).

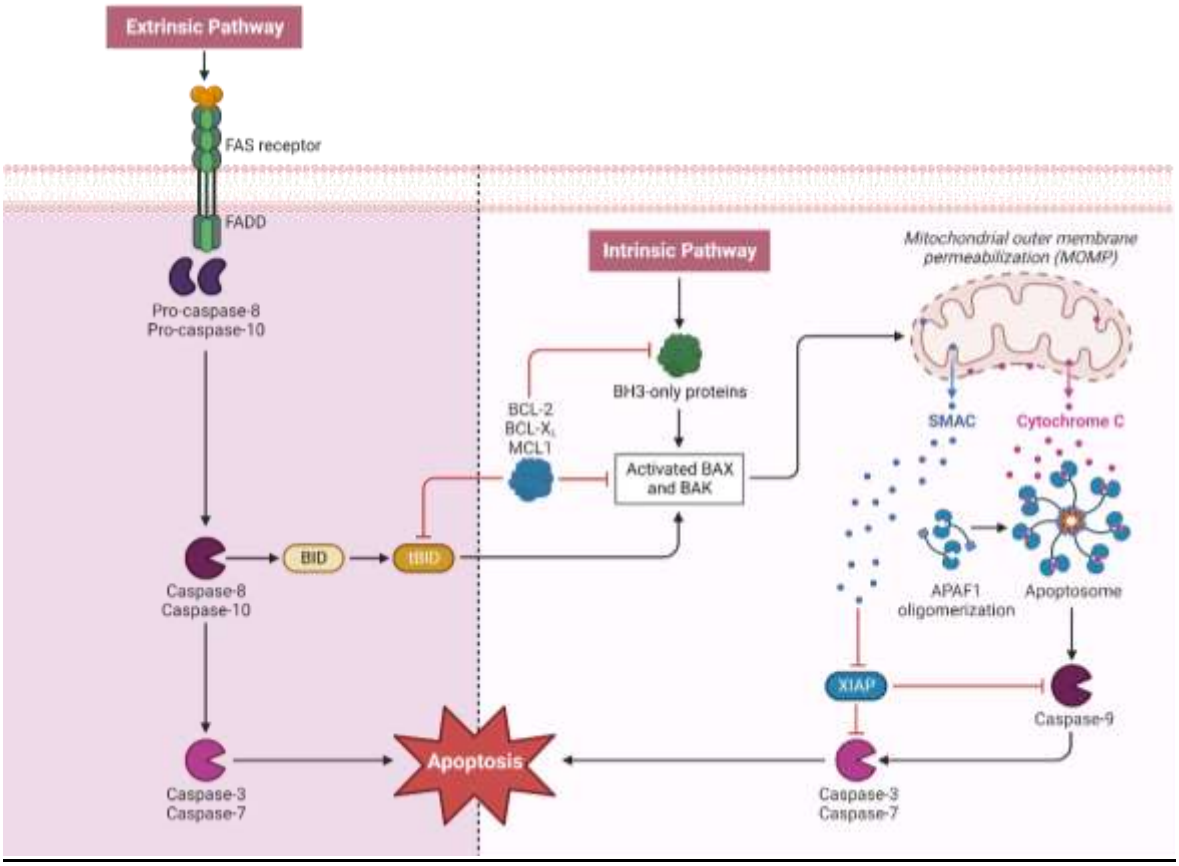

Figure 1. Extrinsic and Intrinsic Pathways of Apoptosis Overview

1.2 Caspase Functions in Cell Death

Caspases, classified as protease enzymes, feature a catalytic cysteine residue in their active site, which plays a critical role in cleaving peptide bonds at specific recognition sites that contain aspartic acid residues, orchestrating peptide activation or inactivation [4]. Caspases can be divided into two main subdivisions: initiator caspases (such as caspases 8, 9, and 10) and executioner caspases (including caspases 3, 6, and 7)[5]. Initiator caspases are activated early in the apoptotic cascade and play a crucial role in initiating the apoptotic process. They activate downstream executioner caspases, which carry out the final stages

of apoptosis by cleaving specific substrates, leading to cellular dismantling and eventual cell death.

The activation of caspases is tightly regulated through various mechanisms. These mechanisms include the expression levels of caspases and their regulators, post-translational modifications such as phosphorylation and ubiquitination, as well as interactions with other cellular factors like inhibitor of apoptosis proteins (IAPs) (**Figure 2**)[6]. These regulatory processes ensure proper control and coordination of caspase activation, allowing cells to execute apoptosis in a controlled and regulated manner.

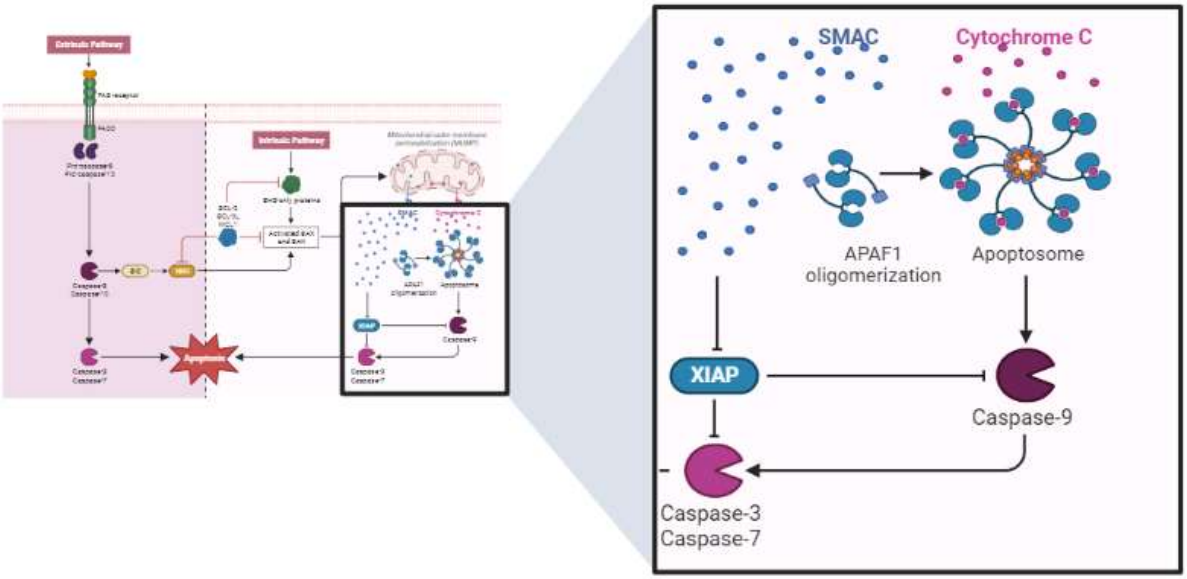

Figure 2. Zoomed-in view of apoptosis: SMAC, XIAP, and effector caspases

1.3 Inhibitor of Apoptosis Protein (IAP)

The initial discovery of the Inhibitor of Apoptosis (IAP) family revealed their role in safeguarding infected cells against apoptosis and enhancing viral replication. This phenomenon was first observed in baculovirus and has since been identified as a conserved mechanism across various species, spanning from yeast to mammals [7-9]. Baculovirus IAP repeat (BIR) domains, 70-80 amino acid sequences that form globular structures with alpha-helices and beta-strands within IAP protein structure, play a pivotal role in anti-apoptotic functions[10, 11]. By inhibiting or promoting caspase degradation, IAP BIR domains play a critical role in determining cell fate and apoptosis (**Table 1**). Their significance extends to cancer biology, as increased expression of IAPs has been associated with enhanced cancer cell survival and resistance mechanisms[12].

Within the Inhibitors of Apoptosis (IAPs) family, the X-chromosome-linked inhibitor of apoptosis protein (XIAP) stands out due to its intricate involvement in cellular signaling pathways, particularly its direct regulation of the caspase cascade[13-15]. Specifically, XIAP plays a role in suppressing both initiator caspase-9 and effector caspase-3 and caspase-7, which are pivotal components of the apoptotic pathway [16-20]. Notably, the XIAP BIR3 domain, distinguished by its compact size, has been identified as the key region responsible for inhibiting caspases, setting it apart from the BIR1-2 domains [21]. Through its binding interface, the XIAP BIR3 domain interacts with a short amino acid sequence in caspase-9 called the IAP-binding motif (IBM), leading to caspase-9

homodimerization. This interaction is stabilized by hydrogen bonds and hydrophobic interactions, resulting in caspase-9 adopting a monomeric zymogen state incapable of initiating downstream apoptotic activation[20].

The ability of XIAP to effectively impede apoptosis at the downstream effector phase, where multiple signaling pathways converge, highlights its significant relevance as a potential target for cancer therapeutics. This significance is further underscored by the observed heightened expression of XIAP in a wide range of tumor cells and cancer specimens[22-24].

Table 1. Inhibitor of Apoptosis family nomenclature, common name, and corresponding caspase

NOMENCLATURE	COMMON NAME	CASPASE SPECIFICITY
BIRC1	NAIP	Caspase-3, -7
BIRC2	cIAP-1	Caspase-3, -7, and -9
BIRC3	cIAP-2	Caspase -3, -7, and -9
BIRC4	XIAP	Caspase-3, -7, and -9
BIRC5	Survivin	Caspase-3, -7
BIRC6	BRUCE/Apollon	Caspase-3, -7
BIRC7	ML-IAP/Livin	Caspase-3, -7, and -9
BIRC8	ILP2	Caspase-9

1.4 Secondary Mitochondria-Derived Activator of Caspase (SMAC)

The initiation phase of apoptosis serves as the trigger for a cascade of events that lead to the activation of caspases, pivotal enzymes involved in the execution of programmed cell death. During this process, the release and subsequent activation of caspases are facilitated. Following the initiation phase, the execution/effector phase of apoptosis ensues, which involves the mitochondria releasing a protein called the secondary mitochondria-derived activator of caspases (SMAC). This endogenous molecule functions as a competitive inhibitor of IAPs, effectively disrupting their anti-apoptotic effects[25]. Once SMAC is liberated into the cytosol, it interacts specifically with a tetrapeptide motif located at the N-terminal region of IAPs. This interaction leads to the release of caspases from the inhibitory influence of IAPs. Notably, the tetrapeptide motif selectively engages with the BIR3 domain of XIAP, a prominent member of the IAP family. As a consequence, caspase-9 is liberated from XIAP's grasp, allowing it to undergo activation. Moreover, this liberation of caspase-9 promotes the assembly of catalytically active caspase-9 homodimers, which are crucial for the execution of apoptotic processes[25-28].

1.5 SMAC Mimetics (SM)

SMAC mimetics (SM) have become a promising development in oncology research due to selectivity, mechanism of action, synergistic effects, broad anticancer activity, and ability to overcome drug resistance. The evolutionarily conserved tetrapeptide binding sequence, represented by AϕPϕ, where ϕ represents a hydrophobic residue, serves as a critical interaction point between

SMAC mimetics and IAPs[3]. The evolutionarily conserved SMAC tetrapeptide binding sequence to the IAP family has specifically captured attention, fostering interest in developing peptidomimetic SMAC compounds for cancer treatment[29, 30]. This binding sequence interaction disrupts the inhibitory function of IAPs, leading to the release of caspases and the re-establishment of apoptotic activity in cancer cells.

Present day SM undergoing clinical trials utilize peptidomimetics via a reversible inhibition mechanism of action. The flexibility of reversible inhibition allows control of off-target effects and target pathway for a tailored treatment strategy while minimizing unwanted effects on normal cellular functions. However, SMs have exceptional selectivity and efficacy on tumor cell receptors[31, 32]. This targeted approach offers the potential for more precise and efficient cancer treatment strategies, minimizing damage to healthy cells and reducing adverse side effects.

In terms of composition, SM can be subdivided as monovalent, characterized by a single tetrapeptide binding sequence, and bivalent, featuring two tetrapeptide binding sequences[33]. Bivalent SM are theorized to exhibit higher binding affinity compared to monomeric SMs[34]. Birinapant is the only documented bivalent reversible SM undergoing clinical trials. However, clinical trials have not yet observed a similarly higher potency of bivalent SM in comparison to monovalent SM[35]. Xevinapant and LCL161 are current

monovalent reversible SM undergoing clinical trials. LCL161 has shown Cytokine release syndrome as a dose-limiting toxicity[34].

SM optimal for XIAP BIR3. “As discussed, SMAC peptides that utilize XIAP as an IAP of interest whilst focusing on targeting the BIR3 domain of XIAP are most favorable as direct inhibitors of downstream caspases[36]

<u>Table 2</u>. SMAC Mimetic Name and Chemical Structure

SMAC Mimetic	Compound Structure
142D6	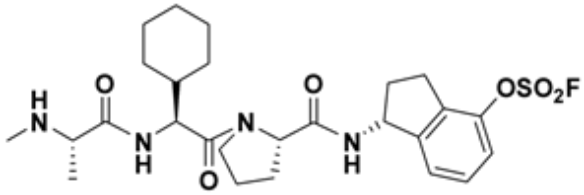
LCL161	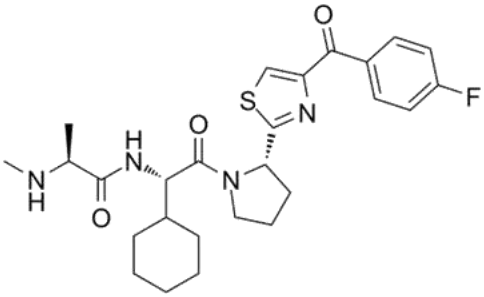
Xevinapant (formerly AT-406 or Debio 1143)	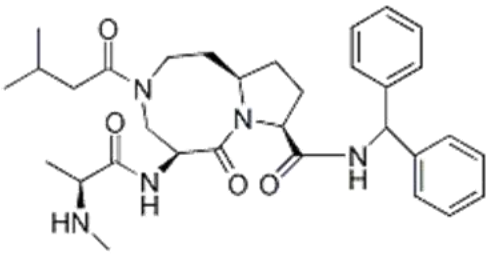
TL32711 (Birinapant)	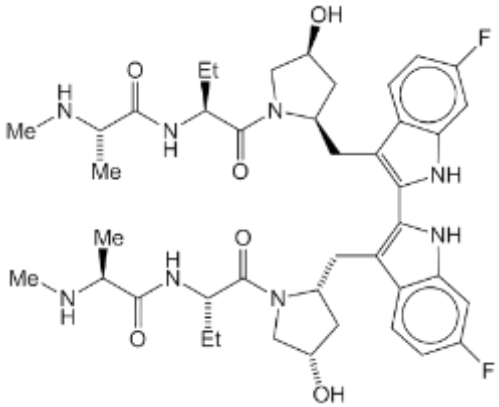

1.6 Novel Aryl-Fluorosulfate Lysine Covalent Inhibitor of Apoptosis Protein (IAP) Antagonist 142D6

Synthesis of SMAC mimetic, (SM) (R)-1-((S)-1-((S)-2-cyclohexyl-2-((S)-2-(methylamino) propanamido) acetyl) pyrrolidine-2-carboxamido) -2,3-dihydro-1H-inden-4-yl sulfurofluoridate, also known as 142D6, has demonstrated new avenues in cancer therapeutics by targeting lysine residues with a aryl-fluorosulfate warhead through irreversible inhibition[37, 38]. Previous research from Pellecchia et al. evaluated biochemical and biophysical assays for potential covalent adduction within the XIAP BIR3 domain[37, 39]., including DELFIA, ΔT_m-induced denaturation thermal shifts (>30°C), SDS gel electrophoresis, and mass spectrometry.

The development of covalent compounds in SMAC research has primarily focused on utilizing cysteine residues. The thiol side group (-SH) of cysteines has been the main target in SMAC development, with the reversible disulfide bond playing a significant role as a stabilizing mechanism[40]. However, it is worth noting that cysteines are one of the least abundant amino acids[41].

Although covalent inhibitors have historically raised safety concerns due to their potential for generalized toxicity, the considerable potency and selectivity of compounds like 142D6 enable the use of lower drug dosages, thereby reducing the risk of toxicity[42, 43]. Orthosteric covalent compounds, such as 142D6, exhibit high affinity and selectivity, which are often viewed as advantageous due to their ability to achieve desired effects at lower doses and their correlation with reduced toxicity[44].

Cancer remains one of the most daunting challenges confronting humanity, causing immense suffering and loss of life. There is an urgent need for innovative therapeutic approaches to surpass the limitations of current treatments[45]. Among the emerging frontiers in cancer research, covalent SMAC mimetics have garnered significant attention for their potential to revolutionize cancer therapy. These compounds operate through a unique cellular mechanism of action and have shown promising results in preclinical studies[46]. However, little is known about how lysine covalently modifying SMAC mimetics, like 142D6, are recognized by XIAP BIR3 domains and specifically inhibit this protein's function. This has hindered the advancement of 142D6 along with advanced pre-clinical optimization of it and its scaffold. Here, we obtain atomic level insights into the covalent inhibition of XIAP BIR3 by SMAC mimetic 142D6. This sheds light on the key XIAP BIR3 142D6 interactions that underpin the inhibitory properties of 142D6. In doing so, we can pave a way forward for lysine covalently modifying XIAP BIR3 targeted therapies that selectively induce cancer cell death while sparing healthy cells.

RESULTS

Pellecchia et al. demonstrated desirable reactivity, plasma stability, cell permeability, and formation of a covalent adduct between 142D6 and XIAP BIR3[37, 47]. Recent biochemical and biophysical studies employing the dissociation-enhanced lanthanide fluorescence immunoassay (DELFIA) displacement assay have revealed compelling evidence of a swift and highly effective interaction between the XIAP BIR3 domain and 142D6. Additionally, Western blot analysis demonstrated cellular permeability of the SMAC mimetic within a transfected cell line. Cellular and *In Vivo* pharmacology studies reported promising longevity (several hours), solubility, plasma stability, potency, and oral bioavailability (F_{PO} 36%). The structural characterization of 142D6 through X-ray crystallography offered concrete evidence 142D6's aryl-fluorosulfate warhead mechanism of action along with electrostatic, hydrophobic, and intermolecular hydrogen bonding interactions with XIAP BIR3, X-ray crystallography was employed[38]. To this end, XIAP BIR3 with amino acid range 253-345 was expressed, and purified. After treatment with 142D6, the XIAP BIR3 142D6 covalent adduct complex was screened against a range of NeXtal precipitant screens using a TTP Labtech Mosquito. Initial crystals were observed in both NeXtal PEGS II and Classics screening suites. Optimization of crystal conditions provided a high-resolution X-ray diffraction data set with a resolution of 1.75 Å from crystals grown in 35% isopropanol and 18% PEG 4000 (**Table 3**). Molecular

replacement using the XIAP BIR3 (PDB 5C0K) as a search model yielded a solution in the space group $P2_12_12_1$.

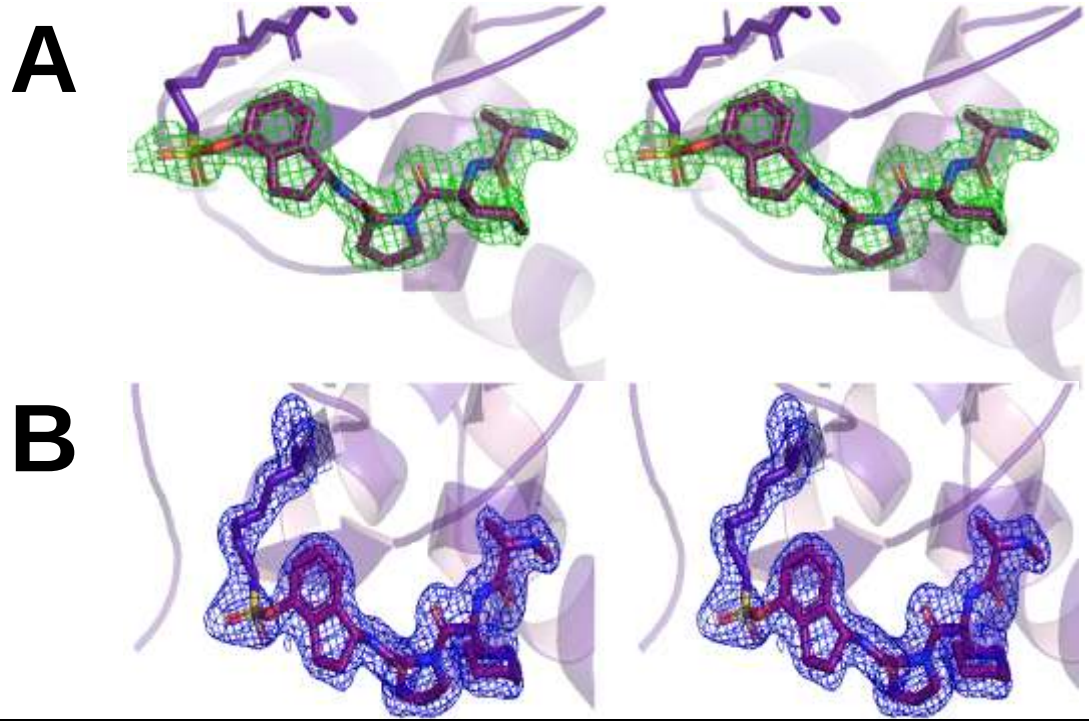

Figure 3. Wall-eyed stereo view of 142D6 covalently linked to XIAP BIR3. The position of K299 and 142D6 are rendered in stick form and colored in purple and magenta, respectively. Green mesh is the F_o-F_c density rendered at 3σ from a composite omit map. Blue mesh is the $2F_o$-F_c density rendered at 1 σ from a composite omit map.

Upon closer examination of both XIAP BIR3 monomers in the asymmetric unit, well-defined F_o-F_c composite omit map density was readily observed and suggesting the placement of the tetrapeptide 142D6 in the region of the BIR3 pocket (Figure 3A). Subsequent structural refinement confirmed the binding pose of 142D6 within this BIR3 pocket via its fit within the resulting $2F_o$-F_c density map (Figure 3B). Globally, as expected, 142D6 spanned across XIAP BIR3 P1-P4

pockets. Unexpectedly, both the F_o-F_c composite omit map and subsequent $2F_o$-F_c density highlighted that 142D6 covalently modified K299, not K297 as postulated (**Figure 3**)[37].

2.1 P1 Pocket

The XIAP BIR3 binding groove is divided into four pockets (P1, P2, P3, and P4), with each pocket interacting with different amino acid caspase residues. Analysis of localized interactions revealed the N-methyl-L-alanine moiety of 142D6 established a hydrogen bond network with the sidechains of Asp310, Glu314, Gln319, and Trp323, spanning across the P1 and P3 interfaces (**Figure 5**). Notably, the Ala1 residue, with its amino group (−NH2), established four strong hydrogen bonds with neighboring residues in BIR3 (Glu314, Gln319, Trp310). Of particular significance was the observation that the Trp310 residue in the P1 pocket of XIAP BIR3 displayed tight hydrophobic interactions exclusively with small, naturally occurring L-configuration residues. Given its favorable binding affinity, hydrophobic nature, and appropriate size, alanine emerged as the ideal candidate for this position[48]. Thus, alanine was selected as the amino acid to occupy this crucial site in the design of 142D6.

Furthermore, the carbonyl group of alanine formed a stabilizing hydrogen bond with the indole NH group of Trp323, further augmenting the interaction between 142D6 and XIAP BIR3. In addition, the backbone carbonyl group (−C═O) of Ala1 formed an additional hydrogen bond with the indole NH group of

Trp323. These interactions contribute to the overall stability and binding activity of the complex.

In summary, the crystallographic analysis of 142D6 within the P1 site of XIAP BIR3 unveiled specific interactions, highlighting the importance of the methyl group localization, hydrogen bond network, and hydrophobic interactions facilitated by alanine. These findings provide insights into the structural basis of the interaction between 142D6 and XIAP BIR3, contributing to our understanding of the binding mechanism and design principles for SMAC mimetics.

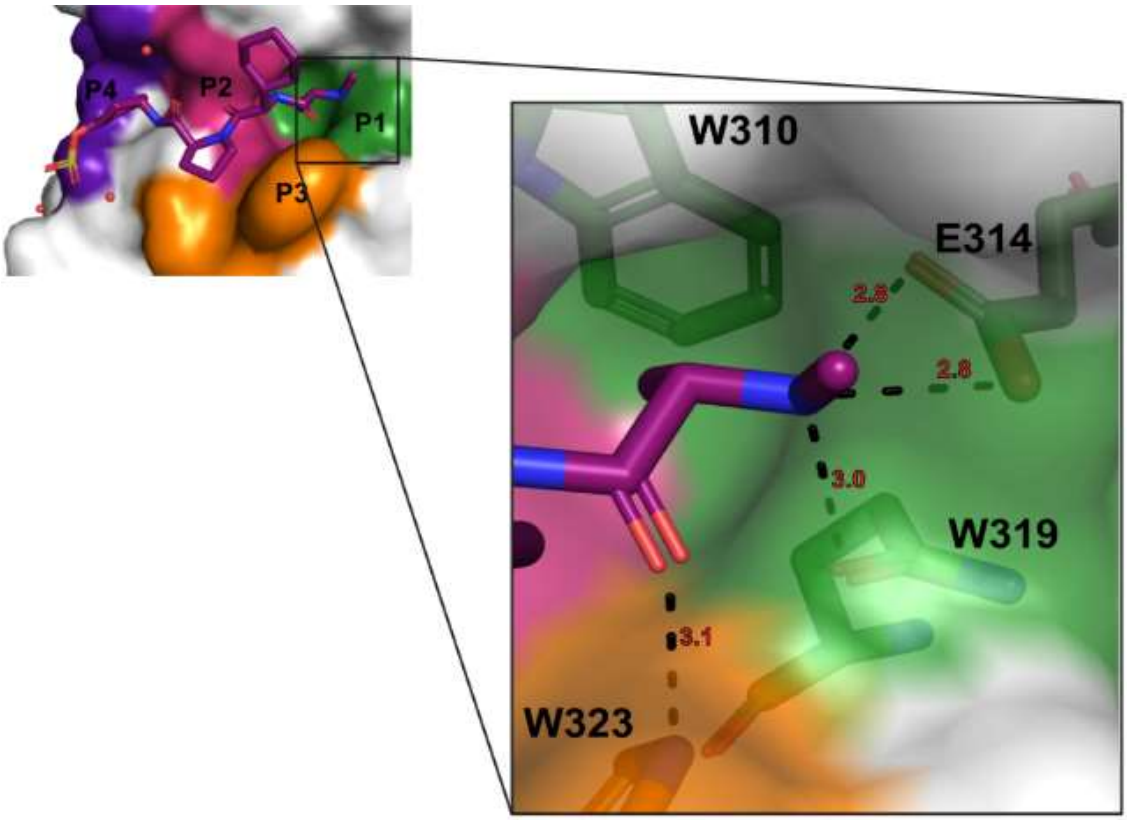

Figure 4. XIAP BIR3 P1 pocket interactions with 142D6. The black dashes represent hydrogen bonds, while distances (Å) are in red. Hydrophobic interactions are observed with W310.

2.2 P2 Pocket

The shallow P2 pocket of XIAP BIR3 has preference for a small, L-configured hydrophobic moiety. The L-cyclohexyl glycine of 142D6 provides optimal arrangement of the side chain for intermolecular hydrogen bonding while minimizing steric hindrance due to its conformational flexibility (**Figure 6**). The engagement with the P2 site primarily relied on a beta-sheet-like hydrogen bonding network. Specifically, the carbonyl and amine groups of 142D6's L-cyclohexyl glycine formed hydrogen bonds with the main-chain amine of Leu307 and the carbonyl of Thr308, respectively. Furthermore, at the P2 site, the cyclohexyl side chain of 142D6 extended towards the bulk solvent, taking advantage of a hydrophobic surface provided by the P3 residue, Trp323.

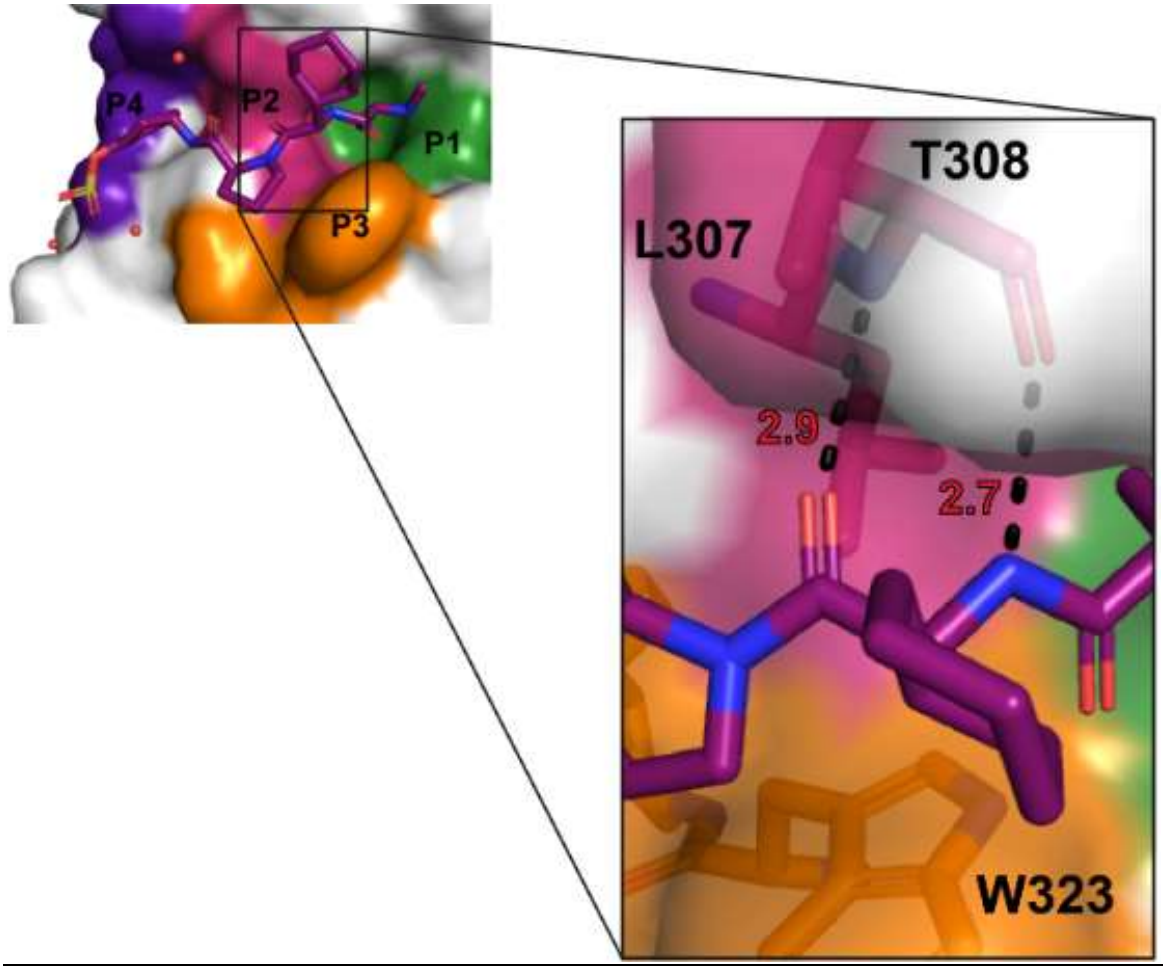

Figure 5. XIAP BIR3 P2 pocket interactions with 142D6. The black dashes represent hydrogen bonds, while distances (Å) are in red. Hydrophobic interactions are observed with W323.

2.3 P3 Pocket

Prior research, in conjunction with the structural examination of 142D6, has yielded valuable insights into the interplay between the XIAP BIR3 P3 pocket and the proline fragment within the tetrapeptide (**Figure 7**)[24, 37]. Proline, with its unique cyclic side chain, has limitations in forming hydrogen bonds but allows for active participation in hydrophobic interactions, particularly with phenylalanine, tyrosine, and tryptophan. The van der Waals interactions create a conformational

environment that accommodates142D6-proline moiety between the Trp323-Tyr324 loop[49]. The π system of Trp323 interacted favorably with the methylene H atoms, further facilitating hydrophobic interactions with the proline moiety of 142D6. The conformation is further stabilized by directing hydrogen bonding between the carbonyl O and the solvent water contralateral to the hydrophobic interactions between proline and residues Trp323 and Tyr324. In summary, the presence of the proline moiety further reinforced the binding and stability of the complex. By strategically utilizing hydrophobic interactions and leveraging the unique properties of proline, the overall binding affinity and stability of the complex were increased.

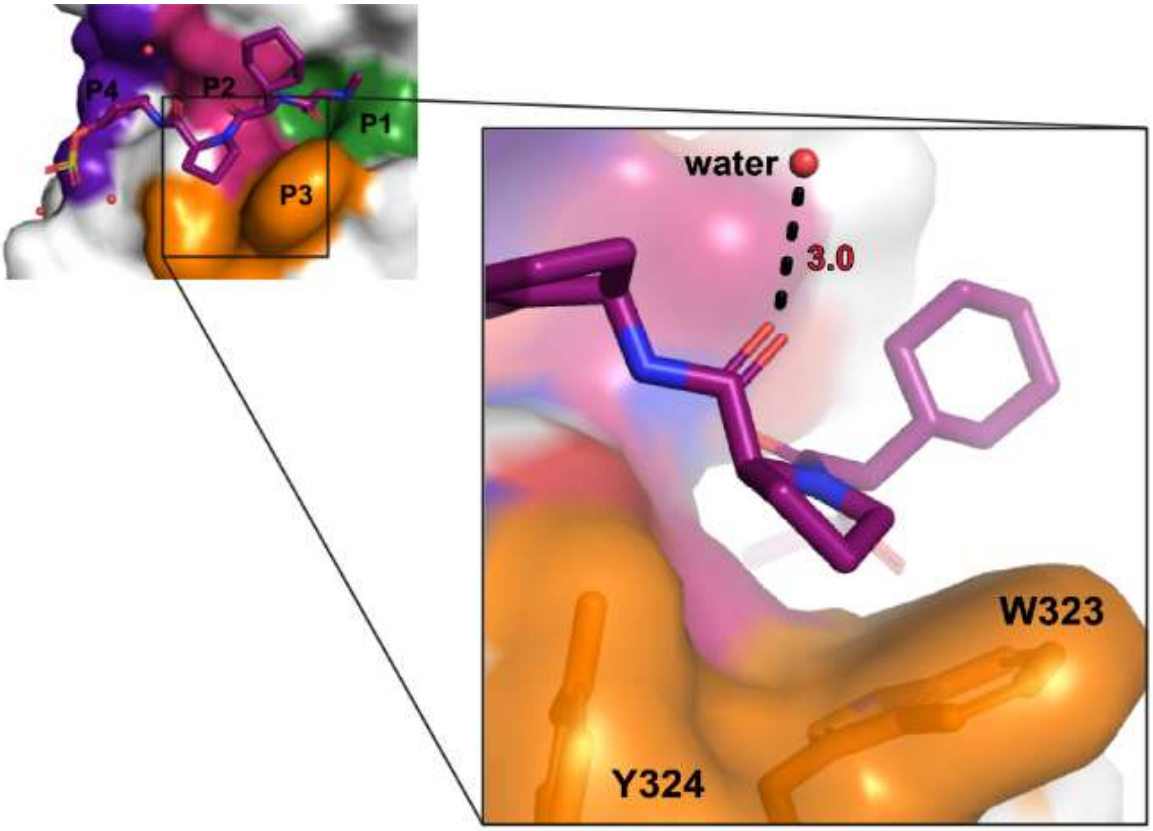

Figure 6. XIAP BIR3 P3 pocket interactions with 142D6. The black dashes represent hydrogen bonds, while distances (Å) are in red. Hydrophobic interactions are observed with W323 and Y324.

2.4 P4 Pocket

Interactions between 142D6 and residues surrounding the P4 site were observed (**Figure 4**). A hydrogen bond was formed between Gly306 and 142D6. Additionally, the amine from the 1-aminoindane moiety of 142D6 inserted itself into a pocket formed by the side chains of Lys297 and Leu292, along with a portion of the main chain in XIAP-BIR3. These interactions played a crucial role in stabilizing the binding at the P4 site. Not only is the covalent interaction between the sulfur of 142D6 and Lys299 present, but the orientation of the sulfamate moiety is also stabilized by a network of hydrogen bonds with

surrounding water molecules. Additionally, the hydrogen bonding network involving the sulfamate moiety of 142D6, water, and the orientation of Arg258 towards 142D6 ensures the secure placement of the SM in the P4 pocket (**Figure 9**).

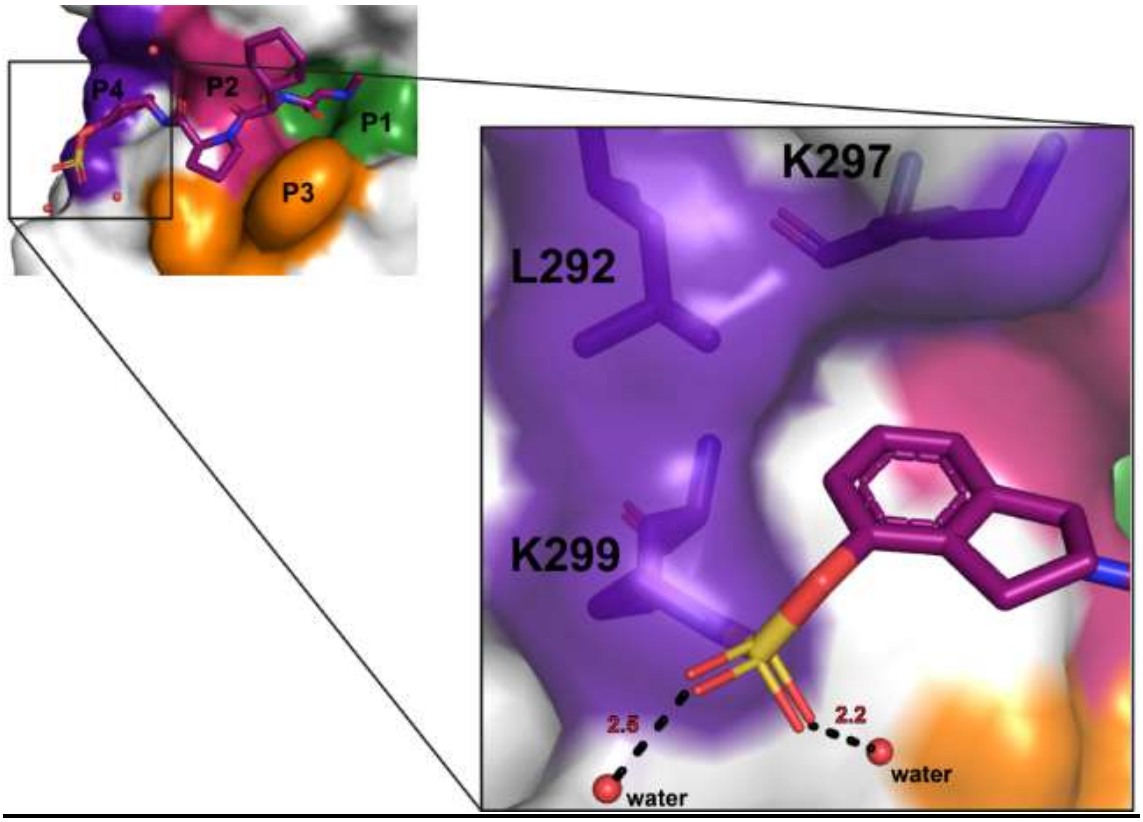

Figure 7. XIAP BIR3 P4 pocket interactions with 142D6. Hydrophobic interactions are observed with L292.

In summary, the binding of 142D6 with the XIAP BIR3 protein involved an intricate network of hydrogen bonds and hydrophobic interactions, particularly at the P1, P2, P3, and P4 sites. The specific interactions included the positioning of the methyl group within the P1 pocket, the engagement with the P2 site through a beta-sheet-like hydrogen bonding network, and the utilization of hydrophobic

surfaces in the P3 and P4 regions. Collectively, these interactions contributed to the stability of the 142D6 XIAP BIR3 interaction.

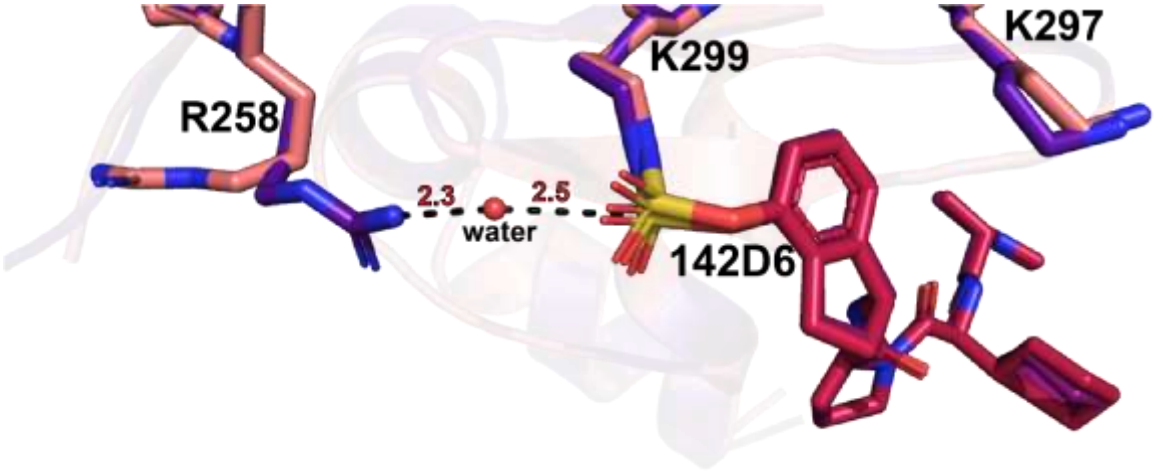

Figure 8. Overlay of monomers A (br3) and B (br7) from the crystal structure of XIAP BIR3-142D6 complex. 142D6 belonging to monomer A are shown in deep salmon and 142D6 belonging to monomer B are shown in br3. The black dashes represent hydrogen bonds, while distances (Å) are in red.

DISCUSSION & CONCLUSIONS

The XIAP BIR3 domain, known for its highly specific binding, participates in multiple protein-protein interactions essential for its association with SMAC and caspase[13-15]. SMAC mimetic (R)-1-((S)-1-((S)-2-cyclohexyl-2-((S)-2-(methylamino) propanamido) acetyl) pyrrolidine-2-carboxamido) -2,3-dihydro-1H-inden-4-yl sulfurofluoridate, commonly known as 142D6, can effectively target the BIR3 domain in a similar fashion by incorporating the AϕPϕ tetrapeptide binding moiety framework and enabling the formation of intricate molecular hydrogen networks, ionic bonding, and hydrophobic interactions[50]. In P2, the (R)-cyclohexyl side chain optical isomerism locks 142D6 by outwardly orienting the

hydrophobic side chain towards the cellular environment, while the carbonyl forms a hydrogen bond with water solvent. At the P4 pocket, the indane ring structure restricts rotational movement of the molecule and creates stability through delocalized pi-bonds.

Not only does 142D6 snugly conform to the BIR3 domain, mirroring the interaction observed between caspase and SMAC, but it also forms a secure covalent bond with a reactive lysine side chain in the P4 pocket. The prevailing theory posits that the reaction is orchestrated via a concerted Substitution with Fluoride Electrophiles (SuFEx) S_N2 mechanism (**Figure 10**). This process entails a nucleophilic XIAP BIR3 lysine engaging with the electrophilic 142D6 aryl fluorosulfate warhead, which is facilitated by the absence of bulky substituents on the aryl fluorosulfate and the proficient leaving group ability of the fluoride (F-) anion [51, 52]. The lysine side chain attack on the aryl-fluorosulfate creates a new covalent bond and displaces the fluoride leaving group, resulting in the substitution of the leaving group with the lysine side chain.

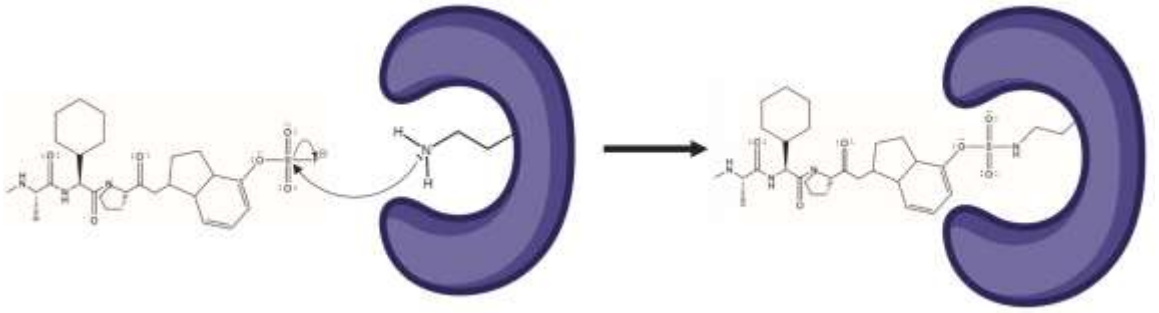

<u>Figure 9.</u> Proposed S_N2 Sulfur (VI) fluoride exchange (SuFEx) reaction mechanism of 142D6 and XIAP BIR3. A concerted reaction in which the XIAP BIR3 lysine side chain residue nucleophile attacks the aryl-fluorosulfate warhead reactant. A covalent adduct of XIAP BIR3 142D6 is synthesized as a product.

In previous research conducted by Pellecchia et al., a hypothesis was postulated that the aryl fluorosulfate moiety of 142D6 could form a covalent bond with Lys297 of XIAP BIR3 based on DELFIA data and MS analyses[37]. However, subsequent analysis utilizing x-ray crystallography to furnish intricate insights into atom positioning, chemical bonding, and overall electronic interactions definitively revealed that the covalent bond is, instead, formed with Lys299.

The alignment of the molecule in the optimal conformation for the reaction was believed to be facilitated by a network of hydrogen bonds, favoring the interaction with Lys299 rather than Lys297 [37, 39]. The covalent bonding of 142D6 to Lys299 is likely advantageous due to the minimization of angle strain in the P4 pocket, making it energetically more favorable compared to the alternative Lys297 (**Figure 8**).

To further elucidate the interactions that position 142D6 in XIAP BIR3, a comparison of the monomer A and monomer B revealed a water-mediated hydrogen bonding network involving Arg258 (**Figure 9**). By participating in this hydrogen bonding network, Arg258 influences electrostatic interactions and increases reactivity of Lys299. The interplay between the arginine, water, and lysine promotes a microenvironment necessary for covalent bond formation with the aryl fluorosulfate warhead of 142D6. These combined interactions contribute

to the high affinity and specificity of 142D6 towards the XIAP BIR3 Lys299, facilitating its potential as a potent therapeutic agent.

3.1 Opportunities for Improved Efficacy of the 142D6 Scaffold

SMAC mimetics (SM) have emerged as a highly promising class of compounds that deserve further research for their potential to revolutionize cancer therapeutics and address critical challenges in current treatment approaches. The favorable reaction rate, cellular permeability, aqueous solubility, and stability, along with the remarkable plasma stability and ligand-protein irreversible interaction observed between 142D6 and XIAP BIR3, provide compelling evidence of the exceptional properties of SM in oncology[37, 38]. By targeting and inhibiting inhibitors of apoptosis proteins (IAPs), SMAC mimetics can reactivate apoptotic pathways and induce cell death in cancer cells, even those that exhibit resistance to conventional therapies. This mechanism of action offers a novel avenue to overcome treatment resistance and improve patient outcomes. Furthermore, SM exhibits the ability to selectively target cancer cells while sparing normal healthy cells, minimizing potential side effects. The favorable results obtained from the extensive study of the properties of SMAC mimetics, including their reaction rate, cellular permeability, aqueous solubility, stability, and ligand-protein interaction, underscore the potential of these compounds in oncology. Continued research in this field holds promise for unlocking the full therapeutic potential of SM, ultimately leading to the

development of more effective and targeted treatments for various types of cancers[35].

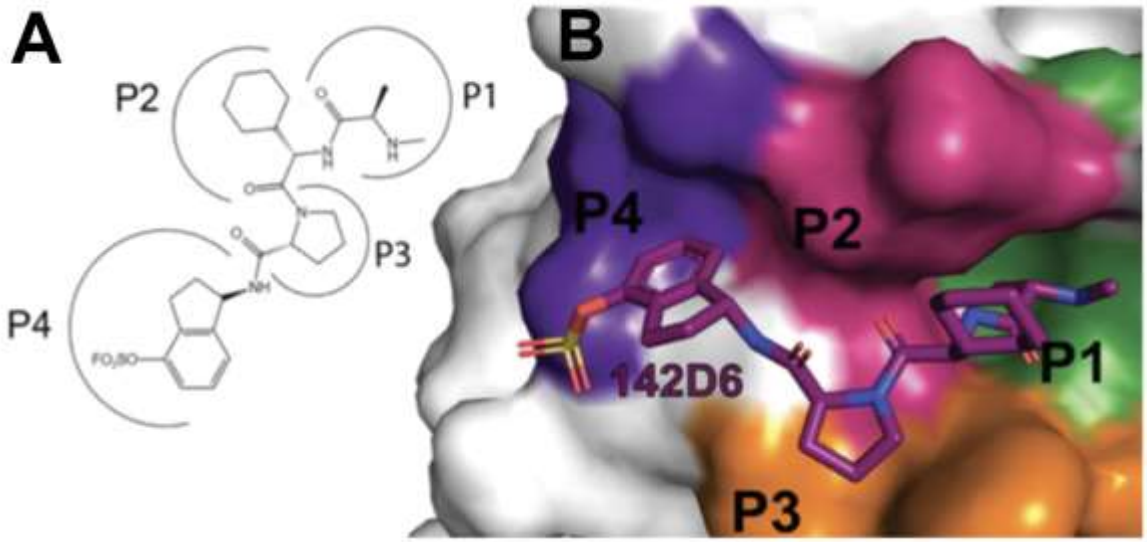

Figure 10. (A) Schematic representation of the interactions of 142D6 in the BIR3 domain pockets of XIAP. (B) Location of 142D6 into the BIR3 binding pocket. The surface of XIAP-BIR3's P1-P4 binding positions a colored respectively as forest, warmpink, orange, and br7.

The promising outcomes stemming from the investigation into the pharmacokinetic and pharmacodynamic properties of SM 142D6 serve as a compelling catalyst in paving the way for potential breakthroughs in cancer therapeutics. These results not only contribute to the growing body of knowledge but also offer new avenues for exploration and advancement in the field of cancer treatment. Dimerization is a common characteristic of proapoptotic protein design development and thus a potential avenue to boost efficacy of 142D6 as a monobivalent or heterobivalent SM[53]. 142D6 as a dimer may further enhance the effect of XIAP on the initiation and effector phases of the apoptotic pathway by affecting both BIR2 and BIR3 domains[54]. Analysis of the XIAP BIR3 142D6 X-ray

crystallography structure is an invaluable tool in the exploration and discovery of potential linker regions for dimerization. The P1 pocket positioning of N-methyl-L-alanine moiety provides an advantageous platform for the implementation of click chemistry reactions (**Figure 5**). The specific conformation and orientation of the 142D6 N-terminus provides an optimal site for the introduction of a dimerization linker region, which allows for proper spacing and flexibility to facilitate effective engagement. Modifications of 142D6 as a dimer may provide comparable selectivity, potency, combination potential, and translational potential of Birinapant.

Similarly, the exploration of heterobivalent SM presents an intriguing opportunity to further optimize the effectiveness of bivalent SMAC mimetics like 142D6. It may be possible to enhance the pro-apoptotic effects by incorporating the ATAA tetrapeptide moiety, which has previously shown high affinity for XIAP BIR2[49]. The combination of 142D6, a linker, and the ATAA moiety that specifically targets XIAP BIR2, can lead to enhanced binding affinity and specificity for inhibiting IAP proteins. This could result in a more robust and targeted disruption of the anti-apoptotic functions of IAP proteins, further promoting apoptotic pathways and improving the induction of cancer cell death. By leveraging the unique characteristics of each component, this compound could offer improved efficacy and selectivity in targeting IAP proteins, thereby enhancing its pro-apoptotic effects. Ultimately, further research and exploration of dimerization of 142D6 may further maximize its specificity, potency, stability,

pharmacokinetic and pharmacodynamic properties, combination potential, and translational potential.

Outside forming dimeric versions of 142D6, **Figure 11** highlights additional areas of possible optimization. The SM 142D6 exhibits promising pharmacokinetic and pharmacodynamic properties, revealing only a few minor possibilities for further optimization. The C-terminus alanine moiety offers a potential network of electrostatic interactions with neighboring Lys311 and Lys322. The XIAP BIR3 nucleophilic residues would allow the addition of a (-(-COOH) carboxylic acid to 142D6. Alternatively, an addition of an (-$ArOSO_2F$) aryl-fluorosulfate warhead to the C-terminus may invoke a covalent bond similar to Lys299 and 142D6. Synthesis of a covalent adduct with Lys311 would be monumental to the specificity of a SM to XIAP BIR3. Downstream, in the second position of the SM tetrapeptide 142D6, the inherent flexibility of the cyclohexyl residue allows a conformational positioning towards the bulk solvent. The proximity of Asp309, a polar, acidic side chain may further increase the intermolecular network with a heterocyclic organic compound such as a ((-$CH_2)_4NH$) pyrrolidine. These strategies may provide opportunities for optimizing the therapeutic applications of 142D6 as a SM for XIAP BIR3.

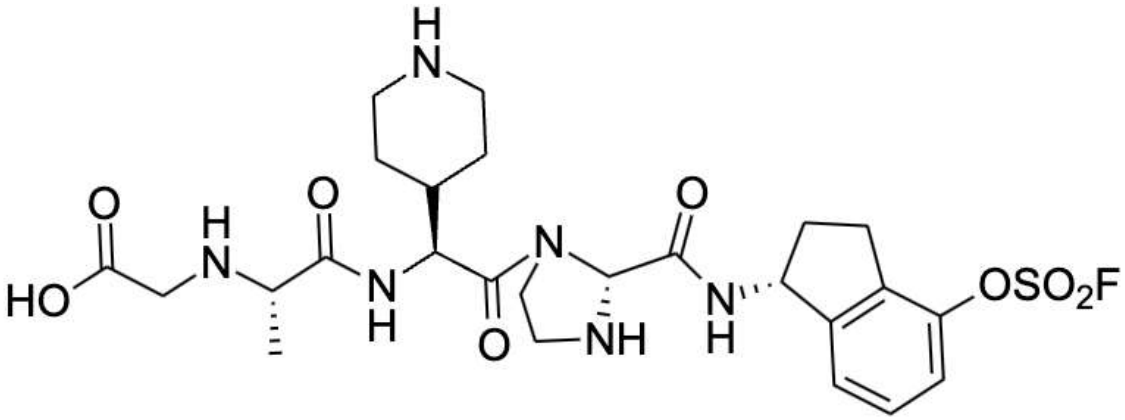

Figure 11. Proposed 142D6 modifications. The C-terminal of a protein includes an additional carboxyl group and the second position cyclohexyl moiety has been substituted for pyrrolidine.

Targeting alternative residues that are available in XIAP BIR3 may provide further opportunities for covalent adduct formation and expand the range of reactivity[37, 39-41, 55]. By exploring the availability of alternative target residues, such as serine, threonine, and tyrosine, researchers can broaden the range of potential interactions[56, 57]. Future investigations should aim to elucidate the specific reactions involving 142D6 and these amino acids within XIAP BIR3. This can be achieved through a comprehensive assessment of the chemical environment, including factors such as pH, nutrient supply, pO2 levels, and heat production species, as well as a thorough investigation of the reaction kinetics[58-60].

3.2 Concluding Thoughts

Tumor microenvironments are characterized by a variety of abnormal features that significantly influence chemical reactions. The complex interplay of factors such as pH, nutrient availability, oxygen tension (pO_2), and heat production species creates a unique chemical landscape within tumors. The acidic pH often observed in tumor microenvironments can impact reaction rates and alter the reactivity of molecules. Furthermore, the limited nutrient supply and altered metabolism within tumors can affect the availability of reactants and the overall energetics of chemical reactions. In addition, the hypoxic conditions, and the production of heat within tumor cells contribute to the intricate tumor microenvironment, influencing thermodynamics and reaction kinetics.

Understanding the impact of tumor microenvironment characteristics on chemical reactions is of utmost importance. Further research should explore the interplay between these factors and the specific reactions involving 142D6 and target residues, such as serine, threonine, and tyrosine, within XIAP BIR3. This can provide valuable insights into the mechanisms underlying the reactivity and covalent adduct formation, ultimately aiding in the development of targeted therapeutic strategies.

EXPERIMENTAL SECTION

4.1 Crystallization of XIAP BIR3 142D6

The XIAP BIR3 142D6 covalent adduct complex was screened against a range of QIAGEN NeXtal suite conditions by the hanging drop format using a TTP Labtech Mosquito (TTP Labtech, Hertfordshire, United Kingdom). In short, XIAP BIR3 142D6 crystals were grown from 15 mg/mL purified protein in 25 mM HEPES (pH 7.6), 50 mM NaCl, 1 mM MgSO2, 0.25 mM TCEP buffer solution by sitting drop vapor diffusion at 20 °C against 2 µL of crystallization precipitant. The polyethylene glycol (PEG) II Suite well number 53 with buffer 0.1 M HEPES pH 7.5 and precipitant 10%(w/v) PEG 4000; 20% (w/v) isopropanol generated crystallization that was further optimized using combinations of 10% to 20% PEG 4000 and 25% to 50% isopropanol gradients. The final optimized crystals were obtained from 35% isopropanol and 18% PEG 4000. The crystals were mounted onto liquid nitrogen flash-cooled nylon loops and flash-cooled in a cryoprotective 142D6 was collected at Advanced Photon Source (Argonne National Labs, Argonne, IL) on SBC-CAT beamline ID-19 using a PILATUS3 X 6M detector.

4.2 Data Processing and Structure Solutions

X-ray images were indexed, integrated, and scaled in the $P2_12_12_1$ space group using the program HKL2000[4]. Experimental phasing was employed using the Phenix suite of programs[61]. To create a cross-validation set from a random 5% of the reflections to be used throughout refinement, the CCP4 software suite was employed[62]. The initial phase solutions were established using molecular

replacement via Phaser with 5c0k[63]. The structure was refined initially using Autobuild then iterative cycles of model building with COOT 0.7.1 and refinement with Phenix[62]. Water molecules were originally added to $2F_o - F_c$ density peaks of >1σ using the Find Water COOT program function and then were assessed individually8. Subsequently, PEG and other ligands were individually placed into structures based on $F_o - F_c$ density at 3σ and refined with Phenix; refined after which the structures are positioned to fit the $2F_o - F_c$ density at 1σ[64]. The final model of each structure was examined via Molprobity to confirm the quality of the structures[65]. The data collection and refinement statistics for each structure are listed in **Table 3**.

Table 3. XIAP BIR3 142D6 complex X-ray Data collection and Refinement Statistics. (Molecular Replacement)

XIAP BIR3 142D6	
Data collection	
Space group	$P2_12_12_1$
Cell dimensions	
a, b, c, (Å)	34.2, 55.2, 93.0
α, β, γ (°)	90, 90, 90
Wavelength	0.97
Resolution (Å)	32.1-1.75 (1.78-1.75)
R_{pim} (%)	59.0 (30.5)
R_{merge} (%)	15.8 (76.3)
$I / \sigma I$	13.37 (1.54)
$CC_{1/2}$	0.972 (0.846)
Completeness (%)	99.2 (98.9)
Redundancy	6.6 (5.7)
Refinement	
Resolution (Å)	32.1 – 1.75
No. reflections	18274 (1771)
R_{work} (%) / R_{free} (%)	17.7 / 20.9
No. atoms	
Protein	1511
Ligand	108
Water	90
B factors	
Protein	31.10
Ligand	39.09
Water	41.0
R.m.s. deviations	
Bond lengths (Å)	0.005
Bond angles (°)	0.71
Ramachandran favored (%)	98.35
Ramachandran allowed (%)	1.65
Ramachandran outliers (%)	0.00

[a] Values in parentheses are for highest-resolution shell. The dataset was collected from a single crystal.

REFERENCES

(1) Lawen, A. Apoptosis-an introduction. *Bioessays* **2003**, *25* (9), 888-896. DOI: 10.1002/bies.10329 From NLM Medline.

(2) Elmore, S. Apoptosis: a review of programmed cell death. *Toxicol Pathol* **2007**, *35* (4), 495-516. DOI: 10.1080/01926230701320337 From NLM Medline.

(3) Fulda, S.; Vucic, D. Targeting IAP proteins for therapeutic intervention in cancer. *Nat Rev Drug Discov* **2012**, *11* (2), 109-124. DOI: 10.1038/nrd3627 From NLM Medline.

(4) Mace, P. D.; Day, C. L. A massive machine regulates cell death. *Science* **2023**, *379* (6637), 1093-1094. DOI: 10.1126/science.adg9605 From NLM Medline.

(5) Fan, T. J.; Han, L. H.; Cong, R. S.; Liang, J. Caspase family proteases and apoptosis. *Acta Biochim Biophys Sin (Shanghai)* **2005**, *37* (11), 719-727. DOI: 10.1111/j.1745-7270.2005.00108.x From NLM Medline.

(6) Riedl, S. J.; Shi, Y. Molecular mechanisms of caspase regulation during apoptosis. *Nat Rev Mol Cell Biol* **2004**, *5* (11), 897-907. DOI: 10.1038/nrm1496 From NLM Medline.

(7) Hu, S.; Vincenz, C.; Buller, M.; Dixit, V. M. A novel family of viral death effector domain-containing molecules that inhibit both CD-95- and tumor necrosis factor receptor-1-induced apoptosis. *J Biol Chem* **1997**, *272* (15), 9621-9624. DOI: 10.1074/jbc.272.15.9621 From NLM Medline.

(8) Fulda, S. Regulation of cell migration, invasion and metastasis by IAP proteins and their antagonists. *Oncogene* **2014**, *33* (6), 671-676. DOI: 10.1038/onc.2013.63 From NLM Medline.

(9) Mace, P. D.; Shirley, S.; Day, C. L. Assembling the building blocks: structure and function of inhibitor of apoptosis proteins. *Cell Death Differ* **2010**, *17* (1), 46-53. DOI: 10.1038/cdd.2009.45 From NLM Medline.

(10) Shu, K.; Iwamoto, N.; Honda, K.; Kondoh, Y.; Hirano, H.; Osada, H.; Ohno, H.; Fujii, N.; Oishi, S. Development of Mirror-Image Screening Systems for XIAP BIR3 Domain Inhibitors. *Bioconjug Chem* **2019**, *30* (5), 1395-1404. DOI: 10.1021/acs.bioconjchem.9b00154 From NLM Medline.

(11) Welsh, K.; Milutinovic, S.; Ardecky, R. J.; Gonzalez-Lopez, M.; Ganji, S. R.; Teriete, P.; Finlay, D.; Riedl, S.; Matsuzawa, S.; Pinilla, C.; et al. Characterization of Potent SMAC Mimetics that Sensitize Cancer Cells to TNF Family-Induced Apoptosis. *PLoS One* **2016**, *11* (9), e0161952. DOI: 10.1371/journal.pone.0161952 From NLM Medline.

(12) Krepela, E.; Dankova, P.; Moravcikova, E.; Krepelova, A.; Prochazka, J.; Cermak, J.; Schutzner, J.; Zatloukal, P.; Benkova, K. Increased expression of inhibitor of apoptosis proteins, survivin and XIAP, in non-small cell lung carcinoma. *Int J Oncol* **2009**, *35* (6), 1449-1462. DOI: 10.3892/ijo_00000464 From NLM Medline.

(13) Kashkar, H. X-linked inhibitor of apoptosis: a chemoresistance factor or a hollow promise. *Clin Cancer Res* **2010**, *16* (18), 4496-4502. DOI: 10.1158/1078-0432.CCR-10-1664 From NLM Medline.

(14) Hanifeh, M.; Ataei, F. XIAP as a multifaceted molecule in Cellular Signaling. *Apoptosis* **2022**, *27* (7-8), 441-453. DOI: 10.1007/s10495-022-01734-z From NLM Medline.

(15) Tamanini, E.; Buck, I. M.; Chessari, G.; Chiarparin, E.; Day, J. E. H.; Frederickson, M.; Griffiths-Jones, C. M.; Hearn, K.; Heightman, T. D.; Iqbal, A.; et al. Discovery of a Potent Nonpeptidomimetic, Small-Molecule Antagonist of Cellular Inhibitor of Apoptosis Protein 1 (cIAP1) and X-Linked Inhibitor of Apoptosis Protein (XIAP). *J Med Chem* **2017**, *60* (11), 4611-4625. DOI: 10.1021/acs.jmedchem.6b01877 From NLM Medline.

(16) Salvesen, G. S.; Duckett, C. S. IAP proteins: blocking the road to death's door. *Nat Rev Mol Cell Biol* **2002**, *3* (6), 401-410. DOI: 10.1038/nrm830 From NLM Medline.

(17) Cummins, J. M.; Kohli, M.; Rago, C.; Kinzler, K. W.; Vogelstein, B.; Bunz, F. X-linked inhibitor of apoptosis protein (XIAP) is a nonredundant modulator of tumor necrosis factor-related apoptosis-inducing ligand (TRAIL)-mediated apoptosis in human cancer cells. *Cancer Res* **2004**, *64* (9), 3006-3008. DOI: 10.1158/0008-5472.can-04-0046 From NLM Medline.

(18) Eckelman, B. P.; Salvesen, G. S.; Scott, F. L. Human inhibitor of apoptosis proteins: why XIAP is the black sheep of the family. *EMBO Rep* **2006**, *7* (10), 988-994. DOI: 10.1038/sj.embor.7400795 From NLM Medline.

(19) Obexer, P.; Ausserlechner, M. J. X-linked inhibitor of apoptosis protein - a critical death resistance regulator and therapeutic target for personalized cancer therapy. *Front Oncol* **2014**, *4*, 197. DOI: 10.3389/fonc.2014.00197 From NLM PubMed-not-MEDLINE.

(20) Shiozaki, E. N.; Chai, J.; Rigotti, D. J.; Riedl, S. J.; Li, P.; Srinivasula, S. M.; Alnemri, E. S.; Fairman, R.; Shi, Y. Mechanism of XIAP-mediated inhibition of caspase-9. *Mol Cell* **2003**, *11* (2), 519-527. DOI: 10.1016/s1097-2765(03)00054-6 From NLM Medline.

(21) Sun, C.; Cai, M.; Meadows, R. P.; Xu, N.; Gunasekera, A. H.; Herrmann, J.; Wu, J. C.; Fesik, S. W. NMR structure and mutagenesis of the third Bir domain of the inhibitor of apoptosis protein XIAP. *J Biol Chem* **2000**, *275* (43), 33777-33781. DOI: 10.1074/jbc.M006226200 From NLM Medline.

(22) Munoz, D.; Brucoli, M.; Zecchini, S.; Sandoval-Hernandez, A.; Arboleda, G.; Lopez-Vallejo, F.; Delgado, W.; Giovarelli, M.; Coazzoli, M.; Catalani, E.; et al. XIAP as a Target of New Small Organic Natural Molecules Inducing Human Cancer Cell Death. *Cancers (Basel)* **2019**, *11* (9). DOI: 10.3390/cancers11091336 From NLM PubMed-not-MEDLINE.

(23) Schimmer, A. D.; Dalili, S.; Batey, R. A.; Riedl, S. J. Targeting XIAP for the treatment of malignancy. *Cell Death Differ* **2006**, *13* (2), 179-188. DOI: 10.1038/sj.cdd.4401826 From NLM Medline.

(24) Cong, H.; Xu, L.; Wu, Y.; Qu, Z.; Bian, T.; Zhang, W.; Xing, C.; Zhuang, C. Inhibitor of Apoptosis Protein (IAP) Antagonists in Anticancer Agent Discovery: Current Status and Perspectives. *J Med Chem* **2019**, *62* (12), 5750-5772. DOI: 10.1021/acs.jmedchem.8b01668 From NLM Medline.

(25) Du, C.; Fang, M.; Li, Y.; Li, L.; Wang, X. Smac, a mitochondrial protein that promotes cytochrome c-dependent caspase activation by eliminating IAP inhibition. *Cell* **2000**, *102* (1), 33-42. DOI: 10.1016/s0092-8674(00)00008-8 From NLM Medline.

(26) Verhagen, A. M.; Ekert, P. G.; Pakusch, M.; Silke, J.; Connolly, L. M.; Reid, G. E.; Moritz, R. L.; Simpson, R. J.; Vaux, D. L. Identification of DIABLO, a mammalian protein that promotes apoptosis by binding to and antagonizing IAP proteins. *Cell* **2000**, *102* (1), 43-53. DOI: 10.1016/s0092-8674(00)00009-x From NLM Medline.

(27) Wu, G.; Chai, J.; Suber, T. L.; Wu, J. W.; Du, C.; Wang, X.; Shi, Y. Structural basis of IAP recognition by Smac/DIABLO. *Nature* **2000**, *408* (6815), 1008-1012. DOI: 10.1038/35050012 From NLM Medline.

(28) Martinez-Ruiz, G.; Maldonado, V.; Ceballos-Cancino, G.; Grajeda, J. P.; Melendez-Zajgla, J. Role of Smac/DIABLO in cancer progression. *J Exp Clin Cancer Res* **2008**, *27* (1), 48. DOI: 10.1186/1756-9966-27-48 From NLM Medline.

(29) Oost, T. K.; Sun, C.; Armstrong, R. C.; Al-Assaad, A. S.; Betz, S. F.; Deckwerth, T. L.; Ding, H.; Elmore, S. W.; Meadows, R. P.; Olejniczak, E. T.; et al. Discovery of potent antagonists of the antiapoptotic protein XIAP for the treatment of cancer. *J Med Chem* **2004**, *47* (18), 4417-4426. DOI: 10.1021/jm040037k From NLM Medline.

(30) Zhou, L. The 'unique key' feature of the Iap-binding motifs in RHG proteins. *Cell Death Differ* **2005**, *12* (8), 1148-1151. DOI: 10.1038/sj.cdd.4401637 From NLM Medline.

(31) Chiangjong, W.; Chutipongtanate, S.; Hongeng, S. Anticancer peptide: Physicochemical property, functional aspect and trend in clinical application (Review). *Int J Oncol* **2020**, *57* (3), 678-696. DOI: 10.3892/ijo.2020.5099 From NLM Medline.

(32) Bose, D.; Roy, L.; Chatterjee, S. Peptide therapeutics in the management of metastatic cancers. *RSC Adv* **2022**, *12* (33), 21353-21373. DOI: 10.1039/d2ra02062a From NLM PubMed-not-MEDLINE.

(33) Morrish, E.; Brumatti, G.; Silke, J. Future Therapeutic Directions for Smac-Mimetics. *Cells* **2020**, *9* (2). DOI: 10.3390/cells9020406 From NLM Medline.

(34) Fulda, S. Smac mimetics as IAP antagonists. *Semin Cell Dev Biol* **2015**, *39*, 132-138. DOI: 10.1016/j.semcdb.2014.12.005 From NLM Medline.

(35) Fulda, S. Promises and Challenges of Smac Mimetics as Cancer Therapeutics. *Clin Cancer Res* **2015**, *21* (22), 5030-5036. DOI: 10.1158/1078-0432.CCR-15-0365 From NLM Medline.

(36) Rathore, R.; McCallum, J. E.; Varghese, E.; Florea, A. M.; Busselberg, D. Overcoming chemotherapy drug resistance by targeting inhibitors of apoptosis proteins (IAPs). *Apoptosis* **2017**, *22* (7), 898-919. DOI: 10.1007/s10495-017-

1375-1 From NLM Medline.

(37) Baggio, C.; Udompholkul, P.; Gambini, L.; Salem, A. F.; Jossart, J.; Perry, J. J. P.; Pellecchia, M. Aryl-fluorosulfate-based Lysine Covalent Pan-Inhibitors of Apoptosis Protein (IAP) Antagonists with Cellular Efficacy. *J Med Chem* **2019**, *62* (20), 9188-9200. DOI: 10.1021/acs.jmedchem.9b01108 From NLM Medline.

(38) Udompholkul, P.; Garza-Granados, A.; Alboreggia, G.; Baggio, C.; McGuire, J.; Pegan, S. D.; Pellecchia, M. Characterization of a Potent and Orally Bioavailable Lys-Covalent Inhibitor of Apoptosis Protein (IAP) Antagonist. *J Med Chem* **2023**. DOI: 10.1021/acs.jmedchem.3c00467 From NLM Publisher.

(39) Gambini, L.; Baggio, C.; Udompholkul, P.; Jossart, J.; Salem, A. F.; Perry, J. J. P.; Pellecchia, M. Covalent Inhibitors of Protein-Protein Interactions Targeting Lysine, Tyrosine, or Histidine Residues. *J Med Chem* **2019**, *62* (11), 5616-5627. DOI: 10.1021/acs.jmedchem.9b00561 From NLM Medline.

(40) Zhang, T.; Hatcher, J. M.; Teng, M.; Gray, N. S.; Kostic, M. Recent Advances in Selective and Irreversible Covalent Ligand Development and Validation. *Cell Chem Biol* **2019**, *26* (11), 1486-1500. DOI: 10.1016/j.chembiol.2019.09.012 From NLM Medline.

(41) Bandyopadhyay, A.; Gao, J. Targeting biomolecules with reversible covalent chemistry. *Curr Opin Chem Biol* **2016**, *34*, 110-116. DOI: 10.1016/j.cbpa.2016.08.011 From NLM Medline.

(42) Bauer, R. A. Covalent inhibitors in drug discovery: from accidental discoveries to avoided liabilities and designed therapies. *Drug Discov Today* **2015**, *20* (9), 1061-1073. DOI: 10.1016/j.drudis.2015.05.005 From NLM Medline.

(43) Lonsdale, R.; Ward, R. A. Structure-based design of targeted covalent inhibitors. *Chem Soc Rev* **2018**, *47* (11), 3816-3830. DOI: 10.1039/c7cs00220c From NLM Medline.

(44) Nussinov, R.; Tsai, C. J. The design of covalent allosteric drugs. *Annu Rev Pharmacol Toxicol* **2015**, *55*, 249-267. DOI: 10.1146/annurev-pharmtox-010814-124401 From NLM Medline.

(45) Global Burden of Disease Cancer, C.; Fitzmaurice, C.; Abate, D.; Abbasi, N.; Abbastabar, H.; Abd-Allah, F.; Abdel-Rahman, O.; Abdelalim, A.; Abdoli, A.; Abdollahpour, I.; et al. Global, Regional, and National Cancer Incidence,

Mortality, Years of Life Lost, Years Lived With Disability, and Disability-Adjusted Life-Years for 29 Cancer Groups, 1990 to 2017: A Systematic Analysis for the Global Burden of Disease Study. *JAMA Oncol* **2019**, *5* (12), 1749-1768. DOI: 10.1001/jamaoncol.2019.2996 From NLM Medline.

(46) Wang, G.; Nikolovska-Coleska, Z.; Yang, C. Y.; Wang, R.; Tang, G.; Guo, J.; Shangary, S.; Qiu, S.; Gao, W.; Yang, D.; et al. Structure-based design of potent small-molecule inhibitors of anti-apoptotic Bcl-2 proteins. *J Med Chem* **2006**, *49* (21), 6139-6142. DOI: 10.1021/jm060460o From NLM Medline.

(47) Gambini, L.; Udompholkul, P.; Salem, A. F.; Baggio, C.; Pellecchia, M. Stability and Cell Permeability of Sulfonyl Fluorides in the Design of Lys-Covalent Antagonists of Protein-Protein Interactions. *ChemMedChem* **2020**, *15* (22), 2176-2184. DOI: 10.1002/cmdc.202000355 From NLM Medline.

(48) Sun, H.; Nikolovska-Coleska, Z.; Yang, C. Y.; Qian, D.; Lu, J.; Qiu, S.; Bai, L.; Peng, Y.; Cai, Q.; Wang, S. Design of small-molecule peptidic and nonpeptidic Smac mimetics. *Acc Chem Res* **2008**, *41* (10), 1264-1277. DOI: 10.1021/ar8000553 From NLM Medline.

(49) Lukacs, C.; Belunis, C.; Crowther, R.; Danho, W.; Gao, L.; Goggin, B.; Janson, C. A.; Li, S.; Remiszewski, S.; Schutt, A.; et al. The structure of XIAP BIR2: understanding the selectivity of the BIR domains. *Acta Crystallogr D Biol Crystallogr* **2013**, *69* (Pt 9), 1717-1725. DOI: 10.1107/S0907444913016284 From NLM Medline.

(50) Crisostomo, F. R.; Feng, Y.; Zhu, X.; Welsh, K.; An, J.; Reed, J. C.; Huang, Z. Design and synthesis of a simplified inhibitor for XIAP-BIR3 domain. *Bioorg Med Chem Lett* **2009**, *19* (22), 6413-6418. DOI: 10.1016/j.bmcl.2009.09.058 From NLM Medline.

(51) Barrow, A. S.; Smedley, C. J.; Zheng, Q.; Li, S.; Dong, J.; Moses, J. E. The growing applications of SuFEx click chemistry. *Chem Soc Rev* **2019**, *48* (17), 4731-4758. DOI: 10.1039/c8cs00960k From NLM PubMed-not-MEDLINE.

(52) Mortenson, D. E.; Brighty, G. J.; Plate, L.; Bare, G.; Chen, W.; Li, S.; Wang, H.; Cravatt, B. F.; Forli, S.; Powers, E. T.; et al. "Inverse Drug Discovery" Strategy To Identify Proteins That Are Targeted by Latent Electrophiles As Exemplified by Aryl Fluorosulfates. *J Am Chem Soc* **2018**, *140* (1), 200-210. DOI: 10.1021/jacs.7b08366 From NLM Medline.

(53) Condon, S. M.; Mitsuuchi, Y.; Deng, Y.; LaPorte, M. G.; Rippin, S. R.; Haimowitz, T.; Alexander, M. D.; Kumar, P. T.; Hendi, M. S.; Lee, Y. H.; et al. Birinapant, a smac-mimetic with improved tolerability for the treatment of solid tumors and hematological malignancies. *J Med Chem* **2014**, *57* (9), 3666-3677. DOI: 10.1021/jm500176w From NLM Medline.

(54) Lu, J.; Bai, L.; Sun, H.; Nikolovska-Coleska, Z.; McEachern, D.; Qiu, S.; Miller, R. S.; Yi, H.; Shangary, S.; Sun, Y.; et al. SM-164: a novel, bivalent Smac mimetic that induces apoptosis and tumor regression by concurrent removal of the blockade of cIAP-1/2 and XIAP. *Cancer Res* **2008**, *68* (22), 9384-9393. DOI: 10.1158/0008-5472.CAN-08-2655 From NLM Medline.

(55) Jones, L. H. Emerging Utility of Fluorosulfate Chemical Probes. *ACS Med Chem Lett* **2018**, *9* (7), 584-586. DOI: 10.1021/acsmedchemlett.8b00276 From NLM PubMed-not-MEDLINE.

(56) Pettinger, J.; Jones, K.; Cheeseman, M. D. Lysine-Targeting Covalent Inhibitors. *Angew Chem Int Ed Engl* **2017**, *56* (48), 15200-15209. DOI: 10.1002/anie.201707630 From NLM PubMed-not-MEDLINE.

(57) Narayanan, A.; Jones, L. H. Sulfonyl fluorides as privileged warheads in chemical biology. *Chem Sci* **2015**, *6* (5), 2650-2659. DOI: 10.1039/c5sc00408j From NLM PubMed-not-MEDLINE.

(58) Weber, C. E.; Kuo, P. C. The tumor microenvironment. *Surg Oncol* **2012**, *21* (3), 172-177. DOI: 10.1016/j.suronc.2011.09.001 From NLM Medline.

(59) Vaupel, P. Tumor microenvironmental physiology and its implications for radiation oncology. *Semin Radiat Oncol* **2004**, *14* (3), 198-206. DOI: 10.1016/j.semradonc.2004.04.008 From NLM Medline.

(60) Gillies, R. J.; Raghunand, N.; Karczmar, G. S.; Bhujwalla, Z. M. MRI of the tumor microenvironment. *J Magn Reson Imaging* **2002**, *16* (4), 430-450. DOI: 10.1002/jmri.10181 From NLM Medline.

(61) Adams, P. D.; Afonine, P. V.; Bunkoczi, G.; Chen, V. B.; Davis, I. W.; Echols, N.; Headd, J. J.; Hung, L. W.; Kapral, G. J.; Grosse-Kunstleve, R. W.; et al. PHENIX: a comprehensive Python-based system for macromolecular structure solution. *Acta Crystallogr D Biol Crystallogr* **2010**, *66* (Pt 2), 213-221. DOI: 10.1107/S0907444909052925 From NLM Medline.

(62) Emsley, P.; Cowtan, K. Coot: model-building tools for molecular graphics. *Acta Crystallogr D Biol Crystallogr* **2004**, *60* (Pt 12 Pt 1), 2126-2132. DOI: 10.1107/S0907444904019158 From NLM Medline.

(63) McCoy, A. J.; Grosse-Kunstleve, R. W.; Adams, P. D.; Winn, M. D.; Storoni, L. C.; Read, R. J. Phaser crystallographic software. *J Appl Crystallogr* **2007**, *40* (Pt 4), 658-674. DOI: 10.1107/S0021889807021206 From NLM PubMed-not-MEDLINE.

(64) Terwilliger, T. C.; Grosse-Kunstleve, R. W.; Afonine, P. V.; Moriarty, N. W.; Zwart, P. H.; Hung, L. W.; Read, R. J.; Adams, P. D. Iterative model building, structure refinement and density modification with the PHENIX AutoBuild wizard. *Acta Crystallogr D Biol Crystallogr* **2008**, *64* (Pt 1), 61-69. DOI: 10.1107/S090744490705024X From NLM Medline.

(65) Chen, V. B.; Arendall, W. B., 3rd; Headd, J. J.; Keedy, D. A.; Immormino, R. M.; Kapral, G. J.; Murray, L. W.; Richardson, J. S.; Richardson, D. C. MolProbity: all-atom structure validation for macromolecular crystallography. *Acta Crystallogr D Biol Crystallogr* **2010**, *66* (Pt 1), 12-21. DOI: 10.1107/S0907444909042073 From NLM Medline.